Quantum spin dynamics studied by the nuclear magnetic relaxation of protons in the Haldane-gap system $(CH_3)_4NNi(NO_2)_3$

Takao Goto,* Takuei Ishikawa,[†] and Yoshiyuki Shimaoka

Graduate School of Human and Environmental Studies, Kyoto University, Kyoto 606-8501, Japan

Yutaka Fujii[‡]

Faculty of Engineering, University of Fukui, Fukui 910-8507, Japan

The nuclear spin-lattice relaxation time T_1 of ^1H in the Haldane-gap system $(CH_3)_4NNi(NO_2)_3$ has been measured at the temperatures down to 50 mK in the gapped and gapless phases with an external field H up to 8.5 T. In the gapless phase for $H > H_{C1} = 2.7$ T, the relaxation rate T_1^{-1} exhibited, below about 3 K, a divergent behavior with decreasing temperature. Such a feature is described by an equation, such as $T_1^{-1} \sim T^{-\alpha}$ with $\alpha = 1 - \eta$, where η is the exponent of the power-law decay for the staggered mode of transverse correlation with respect to the distance in the one-dimensional chain. It has been found that the exponent α takes the values around 0.6, which are consistent with the numerical evaluation for $S = 1$ Heisenberg antiferromagnetic linear chain (HALC). This yields evidence for the realization of Tomonaga-Luttinger liquid phase. At very low temperatures, T_1^{-1} changes into a remarkable decrease after taking a round peak, accompanying an appreciable broadening in the NMR spectrum, and the temperature for such a peak has a trend to increase with increasing field. In the gapped phase for $H < H_{C1}$, T_1^{-1} showed an exponential decrease with decreasing temperature. The experimental results were well interpreted in terms of the intrabranch process associated with the scattering of the magnons within each of $S_z = -1$ and +1 branches of the first excited state. Anomalous hump of T_1^{-1} appeared at low fields below 1 T and at low temperatures below 1 K. This was reasonably explained considering the fractional-spin effect in the $S = 1$ HALC.

I. INTRODUCTION

Low-dimensional Heisenberg antiferromagnets with a finite energy gap above the singlet ground state have been subjects of extensive experimental and theoretical works in the past two decades. Among these systems are the $S = 1$ Heisenberg antiferromagnetic linear chain ($S = 1$ HALC or Haldane-gap system), the $S = 1/2$ linear chain with bond alternation (dimerized chain or spin Peierls system), and the $S = 1/2$ two-leg spin-ladder. Particularly, there has been great interest in the spin dynamics of the gapless quantum phase, which is realized in the presence of an external field H between the first and the second critical fields of H_{C1} and H_{C2}. At these critical fields, the magnetization M begins to appear following the destruction of the gap, and reaches the full value, respectively.

Such a gapless phase is described by Tomonaga-Luttinger (TL) liquid model. This model was introduced by Haldane in the magnetic spin system for the $S = 1/2$ Heisenberg Ising spin chain (XXZ-model) subject to an external field[1] in view of the concept studied by Tomonaga[2] and Luttinger[3] for a strictly soluble model in a one-dimensional fermion system with a linear dispersion relation near the Fermi points. An important criterion for the TL liquid phase is characterized by the fact that the gapless incommensurate mode in the longitudinal correlation and the gapless staggered mode in the transverse correlation exhibit power-law decays with critical exponents η and η_z, respectively, which satisfy the relation $\eta \eta_z = 1$.

As for the $S = 1$ HALC and the $S = 1/2$ bond-alternating chain, Sakai and Takahashi verified first, using the numerical

diagonalization, that the relation $\eta \eta_z = 1$ is satisfied for $H_{C1} < H < H_{C2}$.[4,5] Analytical treatments for the TL liquid phases of the gapped systems were developed on bosonization technique by Chitra and Giamarchi for the $S = 1/2$ dimerized and frustrated chains, and the $S = 1/2$ ladder for the fields at H_{C1} and in its vicinity.[6] They found that the characteristic features in these systems do not appear in the magnetization, but appear clearly in the spin-spin dynamical correlation functions. Thus, the NMR relaxation rate governed by the gapless modes may be a useful probe for the study of the TL phase of the gapped quantum system. It has been shown in Ref. 6 that the divergent behavior of $T_1^{-1} \sim T^{-1/2}$ appears at $H = H_{C1}$ for the dimerized and ladder systems. Giamarchi and Tsvelik investigated the correlation functions for the gapless modes in the whole region of the gapless phase for the $S = 1/2$ two-leg ladder with strong intrarung interaction and obtained the same divergent behavior of T_1^{-1} for H close to H_{C1} and H_{C2}.[7]

Experimentally, in the $S = 1/2$ two-leg ladder system $Cu_2(C_5H_{12}N_2)Cl_4$ (abbreviated as CuHpCl),[8] it has been found that the proton relaxation rate is described as $T_1^{-1} \sim T^{-1/2}$ for $H_{C1}(=7.5$ T$) < H < H_{C2}(=13.5$ T$)$.[9] Such a behavior is consistent with the theoretical prediction presented in Refs. 6 and 7, thus yielding evidence for the realization of the TL liquid phase.

Recently, Haga and Suga investigated theoretically the nuclear spin-lattice relaxation for the TL liquid phases in gapped systems, such as $S = 1/2$ two-leg ladder with a diagonal interaction, which corresponds to the exchange Hamiltonian for CuHpCl, and the $S = 1/2$ two-leg ladder, by mapping the corresponding Hamiltonians onto the $S = 1/2$ XXZ chain.[10] By evaluating the Luttinger parameters η and η^z,

and using the results for the numerical calculation on these parameters,[11] it has been found that the temperature dependence of the relaxation rate is described by equation of $T_1^{-1} \sim T^{-\alpha}$ with $\alpha = 1 - \eta$, where η depends appreciably on the system.

It is noted that quite recent inelastic neutron scattering experiment has revealed that CuHpCl may be regarded to be a three-dimensional (3D) interacting system similar to the Shastry-Sutherland model instead of the spin-ladder.[12]

Thus, no experimental evidence has been verified for the TL liquid phase in the Haldane-gap system, although the numerical values for the Luttinger parameters η and $\tilde{\eta}$ have been obtained in Refs. 4 and 5.

The present work is concerned with the nuclear spin-lattice relaxation of proton in the Haldane-gap system $(CH_3)_4NNi(NO_2)_3$ (abbreviated as TMNIN). Previously T_1 of proton was measured using polycrystalline sample below about 2 T in the temperature range above 1.4 K. It was found that the relaxation rate below about 5 K exhibits an exponential decay with decreasing temperature, reflecting the presence of an energy gap for $H < H_{C1}$.[13,14] In the present measurement, which was also done using the polycrystalline sample, the field and temperature ranges were extended up to 8.5 T and down to 50 mK, respectively. The available maximum field is enough larger as compared to the first critical field $H_{C1} \approx 2.7$ T.[15] Thus, a rather wide field range for $H > H_{C1}$ has been covered, though the second critical field $H_{C2} = 30$ T is much higher.[15]

For $H > H_{C1}$, it was found that the temperature dependence of T_1^{-1} exhibits a divergent behavior, which is described by the equation of $T_1^{-1} \sim T^{-\alpha}$ with $\alpha = 1 - \eta$. This resembles the case of CuHpCl. We interpret our experimental results in terms of realization of the TL liquid phase in the Haldane-gap system TMNIN according to the theory presented in Ref. 10 using the numerical values of the exponent η presented in recent calculation by Sakai.[16] At low temperatures below about 1 K, T_1^{-1} changes into a remarkable decrease after taking a round peak, accompanying an appreciable broadening in the NMR spectrum, and the temperature for such a peak has a trend to increase with increasing field.

For the gapped phase, we shall analyze the experimental results according to Sagi and Affleck's theory for the nuclear spin-lattice relaxation in the Haldane-gap system based on the nonlinear σ model.[17] This theory has been applied in Ref. 18 to the case of CuHpCl for interpretation of T_1 of proton for $H < H_{C1}$.

In addition, we have found that there appears an anomalous hump of the relaxation rate at low temperatures in low fields in the gapped state. This is interpreted in terms of the paramagnetic fluctuation of the fractional spins at the ends of $S = 1$ HALC with finite length.

The outline of the present paper is as follows. In Sec. II, we briefly explain the magnetic properties of TMNIN. The experimental results are shown in Sec. III. Section IV is devoted to the analysis for the experimental results for T_1^{-1} in the gapless and gapped states. In Sec. V, we summarize various features in the present relaxation measurements in the field-temperature diagram and discuss the anomalous behavior of T_1^{-1}, which is associated with the fractional-spin effect. The shape of the NMR spectrum is evaluated for the gapless phase. The conclusion is given in Sec. VI.
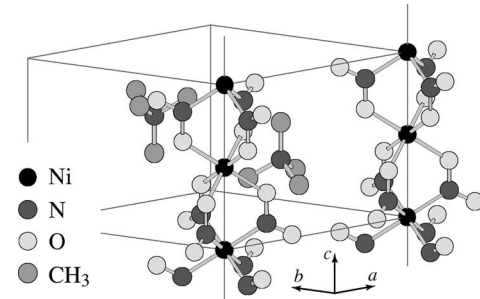
FIG. 1. Crystal structure of TMNIN. The Ni^{2+} linear chains extend along the c axis. The Ni^{2+} ions, which are coordinated octahedrally with six nitrogens or six oxygens, appear alternately. The lattice constants are given in the text.

II. MAGNETIC PROPERTIES

The crystal of TMNIN consists of linear chains of Ni^{2+} ions that extend along the c axis and take hexagonal structure in the ab plane, as shown in Fig. 1. The lattice constants are $a = b = 9.096$ Å and $c = 7.083$ Å. The chain structure is such that the two neighboring Ni^{2+} ions are coordinated octahedrally with six nitrite oxygens or six nitrite nitrogens, alternately, thus both being not chemically identical.[19] This structure has been presented by modifying the first proposal such that adjacent Ni^{2+} ions are bridged by three NO_2 ligands.[13] The $(CH_3)_4N$ ions intervene just in the center of three chains. The exchange interaction and the g value were determined to be $J/k_B = -12$ K and $g = 2.25$ from the analysis of the magnetic susceptibility, and the gap energy has been obtained to be $\Delta/k_B = 4.5$ K.[13] From the high field magnetization measurement at 0.5 K using powder sample, the critical fields were obtained to be $H_{C1} = 2.7$ T and $H_{C2} = 30$ T.[15] The various exchange parameters were later obtained using the oriented crystal as follows; $J_{\parallel}(J_{\perp})/k_B = 10.1$ K (10.4 K), $g_{\parallel}(g_{\perp}) = 2.088(2.091)$, and $H_{C1} = 2.4$ T ($\parallel$) and $H_{C1} = 2.9$ T ($\perp$), where $\parallel$ and $\perp$ represent the cases parallel and perpendicular to the c axis, respectively.[20] The single-ion anisotropy is extremely small as given by the value of $D/k_B = 0.5$ K or 0.03 K.[20]

Heat capacity and susceptibility were measured by Kobayashi *et al.* down to 70 mK under the magnetic field up to 7 T.[21] According to the measurements, the gap, which is open for $H > H_{C1}$, has a trend to increase with increasing field with the value of 1.2 K at H_{C1}, thus the complete disappearance of the gap not having been confirmed. In the following, however, we call the field region above H_{C1} as gapless phase.

III. EXPERIMENTAL RESULTS

The NMR measurement was performed with respect to the protons in $(CH_3)_4N$ ions using standard coherent pulsed-NMR spectrometer. The NMR signal was obtained by a spin-echo pulse sequence, and the spectrum was determined by plotting the echo intensity as a function of the external field at the constant operating frequency. The peak position of the resonance field of the NMR spectrum was almost the same as the free-proton position.

The relaxation time T_1 was measured with respect to the peak position of the spectrum by observing the nuclear magnetization recovery $M(t)$ at the time t after the saturation at $t=0$ attained by the rf-comb pulse. The recovery of normalized nuclear magnetization $m(t)=1-M(t)/M_0$ with M_0 of the thermal-equilibrium magnetization was a single exponential as $m(t)=\exp(-t/T_1)$ at least over more than one decade; thus, the corresponding time-constant T_1 was taken to be the relaxation time. However, at low temperatures below about 2 K and at low fields below 1 T, the exponential recovery held only during the initial short time-interval, and the long-time recovery of $m(t)$ fitted rather well the square-root t curve as $m(t)=\exp(-\sqrt{t/\tau_1})$, which yields another time constant τ_1. Such a feature may be attributed to the appearance of the fractional-spin effect, as discussed in detail in Sec. V.

Figure 2 shows the results of the temperature dependence of the relaxation rate T_1^{-1} over the whole temperature range for the various applied fields above and below H_{C1}. Because of the present experimental condition in the NMR measurement using the dilution refrigerator and ^{3}He-temperature cryostat, it was difficult to adjust the operating resonance frequency completely. However, it turned out that the temperature dependence of T_1^{-1} obtained in the temperature ranges below and above about 1.2 K at slightly different NMR operating frequencies, which corresponds at the most to the difference in the applied field of about 0.3 T, are connected smoothly with each other within the experimental errors. Thus, we plotted in Fig. 2 the experimental results for these measurements using the same symbols. In Fig. 2, the experimental error bars are shown only for a few typical data points. We do so as well in Figs. 4, 6, and 8.

Above about 5 K, T_1^{-1} decreases rather monotonously with decreasing temperature independent of the applied field. Below about 5 K, on the other hand, there appears a distinguished difference in the temperature dependence depending on the applied field. Prominent features appear for $H>H_{C1}$. Below about 3 K, T_1^{-1} exhibits an increase with decreasing temperature, and the temperature range where the increase of T_1^{-1} appears moves to the higher side as the field is increased. Qualitatively T_1^{-1} follows the curve such as $T_1^{-1}\sim T^{-\alpha}$, where the power α takes the values around 0.6. In view of its resemblance to the behavior of T_1^{-1} in CuHpCl,[9] the above feature suggests the realization of the TL liquid phase in TMNIN. At low temperatures, T_1^{-1} shows a remarkable decrease after taking a round peak. The decrease of T_1^{-1} below the peak follows approximately the relation $T_1^{-1}\sim T^4$.

For $1\text{ T}<H<2.5\text{ T}$ ($\approx H_{C1}$), on the other hand, T_1^{-1} falls off exponentially with decreasing temperature. The temperature dependence becomes more moderate as H increases thus reflecting the existence of an energy gap that decreases with increasing field. It is noted that the temperature dependence for $H=1$ T and 0.17 T are almost the same above about 1.5 K, which means that the field dependence of T_1^{-1} diminishes in such a low-field range.

We also find that in the temperature dependence of T_1^{-1} for 1 T, a round hump appears around 0.8 K. As mentioned before, the values of T_1^{-1} that exhibit the hump were taken from the initial short-time recovery of $m(t)$. The detail of the feature of the hump will be discussed in Sec. V in relation to
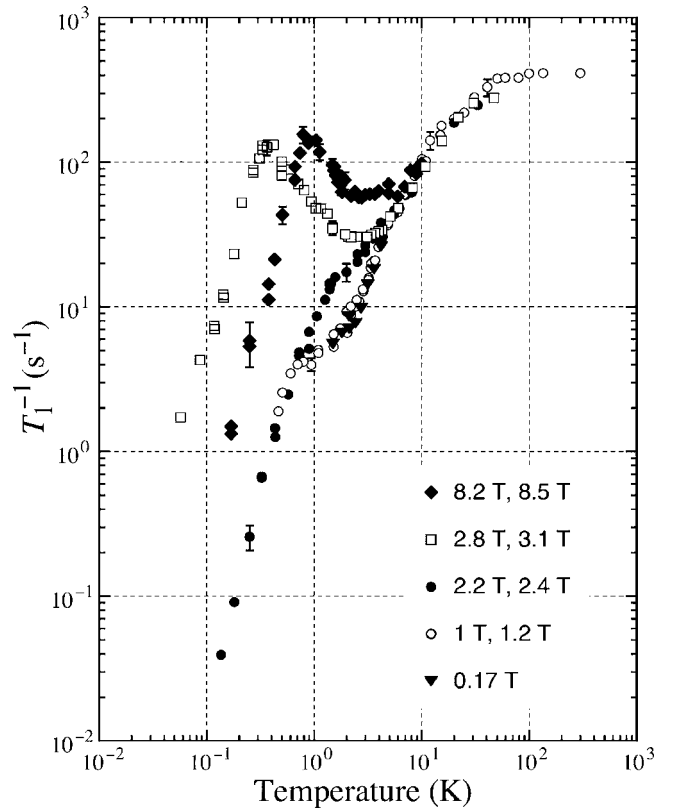
FIG. 2. Temperature dependence of T_1^{-1} for various fields. For the convenience, the data taken in the different temperature ranges with only slightly different operating frequencies were plotted using the same symbol.

effect of paramagnetic fluctuation of the fractional spins of $S=1/2$ at the both ends of the $S=1$ finite linear chain, including the behavior of another time constant τ_1.

Here we refer to the NMR spectrum. Figures 3(a) and 3(b) represent the typical NMR spectra obtained at low temperatures for the gapped and gapless phases, respectively. As seen in Fig. 3(a), the spectrum in the gapped phase is temperature independent down to the lowest temperature. The shape of the spectrum seems to be an asymmetric powder pattern, and as is seen from Fig. 3(b), the spectrum in the gapless phase becomes broad with decreasing temperature. It is noted that such a change of the spectrum begins around the temperature that lies somewhat lower than the temperature where T_1^{-1} takes the round peak. The comparison between the experiment and the calculation for the NMR spectrum is given in Sec. V.

IV. ANALYSIS FOR THE RELAXATION RATES

The nuclear spin-lattice relaxation in the magnetic system is caused by the components of the fluctuating local field at the nuclear site transverse with respect to the quantization axis. In the present case, the proton nuclear spin ($I=1/2$) is coupled to the surrounding Ni^{2+} magnetic moments via the anisotropic dipolar interaction. The effective dipolar interaction is expressed as $\delta\mathcal{H}_{\mathrm{dip}}(t)=g\mu_B\gamma_N\hbar\,\mathbf{I}\Sigma_j\tilde{D}_j\delta\mathbf{S}_j(t)=$
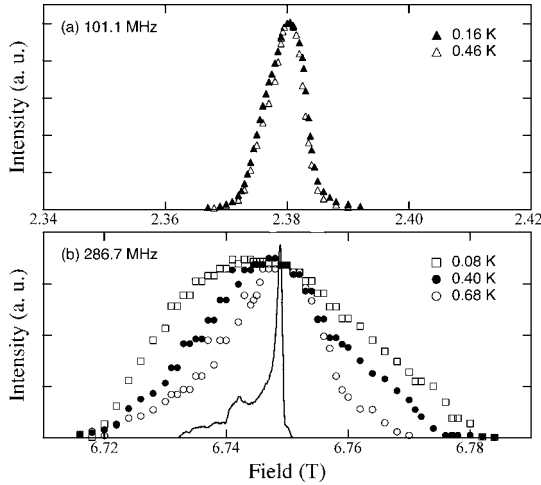
FIG. 3. Examples of NMR spectra for (a) the gapped phase ($H < H_{C1}$) obtained at the operating frequency of $\nu_N = 101.1$ MHz and (b) the gapless phase ($H \gg H_{C1}$) obtained at $\nu_N = 286.7$ MHz. The spectra were obtained by plotting the spin-echo height by changing the applied field H. The solid line in (b) represents the NMR spectra calculated by assuming field-induced uniform moments (see Sec. V).

$-\gamma_N \hbar \mathbf{I} \cdot \delta \mathbf{H}(t)$, where $\widetilde{D}_j$ is the coupling tensor concerning the jth Ni^{2+} spin, and $\delta \mathbf{H}(t)$ represents the fluctuating field at the nuclear site. From now on we take the nuclear quantization axis as the z axis. Then the effective transverse fluctuating fields are expressed as

$$\delta H^{\pm}(t) = - \frac{g \mu_B}{\gamma_N \hbar} \sum_j [D_j^{(\pm, z)} \delta S_j^z(t) + D_j^{(\pm, -)} \delta S_j^-(t) + D_j^{(\pm, +)} \delta S_j^+(t)],$$

$$(1)$$

where $D_j^{(\nu, \nu')}$'s ($\nu = +$, or $-$, and $\nu' = z$, $+$, or $-$) are the components of $\widetilde{D}_j$.

According to the standard perturbation theory, the relaxation rate is given by the Fourier transform at the nuclear Larmor frequency ω_N of the time correlation function $\langle \{\delta H^+(t) \delta H^-(0)\} \rangle$. Using the Fourier-transformed spin variable defined by $\mathbf{S}_q = (1/\sqrt{N}) \Sigma_j \mathbf{S}_j \exp(iqr_j)$, where q is the fluctuating wave vector along the chain, T_1^{-1} is expressed in terms of the longitudinal and transverse dynamical structure factors $S^{z(\perp)}(q, \omega_N)$ as

$$\frac{1}{T_1} = \frac{1}{N} \frac{(g \mu_B \gamma_N)^2}{2} \sum_q [G_q^z S^z(q, \omega_N) + G_q^\perp S^\perp(q, \omega_N)], \quad (2)$$

with

$$S^{z(\perp)}(q, \omega_N) = \int_{-\infty}^{\infty} \langle \{S_{-q}^{z(+)}(t), S_q^{z(-)}\} \rangle \exp(-i\omega_N t) dt, \quad (3)$$

where $G_q^{z(\perp)}$, the geometrical factor, is given as $A_q^{z(\perp)} A_{-q}^{z(\perp)}$ by Fourier transform $A_q^{z(\perp)}$ of the relevant components of $\widetilde{D}_j$. Thus only fluctuating modes, which satisfy the energy-conservation requirement between the electron and nuclear spin systems, are effective under the additional condition

such that the geometrical factors take appreciable values.

Using fluctuation-dissipation theorem, Eq. (3) is expressed in terms of the imaginary part of the dynamical susceptibilities $\chi_{z(\perp)}''(q, \omega_N)$ as

$$S^{z(\perp)}(q, \omega_N) = \frac{2 \chi_{z(\perp)}''(q, \omega_N)}{1 - \exp(\hbar \omega_N / k_B T)}. \quad (4)$$

Since we may put $\hbar \omega_N \ll k_B T$, the relaxation rate is expressed as

$$\frac{1}{T_1} = \frac{2(\gamma_N \mu_B)^2 k_B T}{\hbar} \sum_q \left[G_q^z \frac{\chi_z''(q, \omega_N)}{\omega_N} + G_q^\perp \frac{\chi_\perp''(q, \omega_N)}{\omega_N} \right].$$

$$(5)$$

As for the geometrical factor, the numerical evaluation is difficult in the present case because the direction of the applied field, that is, the nuclear quantization axis, is random with respect to the chain directions in the powder sample, in addition to the fact that the proton position in the $(CH_3)_4N$ ion is not definite. Then in the followings we assume an average constant value for the geometrical factor.

If the paramagnetic fluctuations with $q = 0$ is dominant at high temperatures, Eq. (5) is expressed in terms of the static susceptibility χ_0 as

$$\frac{1}{T_1} \propto T \chi_0. \quad (6)$$

Figure 4 shows the experimental results for T_1^{-1} at low fields of 1.0 and 1.2 T together with the theoretical curve of Eq. (6). This curve, which was normalized at $T = 20$ K, was evaluated using the experimental values of χ_0 given in Ref. 13. Good agreement is found in the high temperatures above 4 K. Thus, it is concluded that the $q = 0$ mode of the paramagnetic fluctuation dominates the relaxation rate at high temperatures in the low field range. In the following, we shall proceed with the low-temperature results.

A. Gapless state

First, we examine the divergent behaviors of T_1^{-1} for $H > H_{C1}$. Sakai and Takahashi studied, numerically, for the $S = 1$ HALC the critical exponents in the following most dominant longitudinal and transverse correlation functions at $T = 0$ K, which correspond to the incommensurate and staggered modes, respectively;[4]

$$\langle S^z(r) S^z(0) \rangle - m^2 = \cos(2k_F r) r^{-\eta_z}, \quad (7a)$$

$$\langle S^x(r) S^x(0) \rangle = (-)^r r^{-\eta}, \quad (7b)$$

where m ($= M/N$) is magnetization per one site, and $2k_F = 2\pi m$ or $\pi - 2\pi m$ for even or odd N, respectively. As mentioned in Sec. I, it has been proved numerically that the exponents η and η^z well satisfy the relation such as $\eta \eta^z = 1$, which certifies the realization of the TL phase.

As given by Eq. (2), the problem for calculating the relaxation rate is reduced to finding the expressions for the time correlation functions $\langle \{S_{-q}^{z(+)}(t), S_q^{z(-)}\} \rangle$. In the cases of the
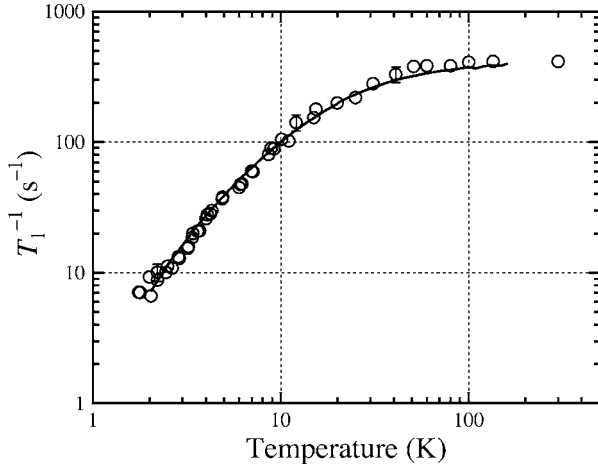
FIG. 4. The temperature dependence of T_1^{-1} for $H=1.0$ and 1.2 T, and $T>1.5$ K. The solid line represents the best fit of Eq. (6) to the experimental results obtained using the experimental values of χ_0 and normalized at $T=20$ K.

$S=1/2$ dimerized chain and the $S=1/2$ ladder, the corresponding Hamiltonians are mapped onto the $S=1/2$ XXZ model. Then the time correlation functions at $T=0$ K are given by the equations that are obtained by replacing r in the power-decay terms in Eqs. (7a) and (7b) by the distance $r=\sqrt{x^2+(v\tau)^2}$ defined in the space-time plane, where x is the real distance along the chain and the ladder, τ is time, and v is the velocity of the elementary excitation at $T=0$.[6,7] These correlation functions are then extended to the finite temperature by the following conformal mapping:

$$v\tau \pm ix = \frac{v}{\pi T}\sin\frac{\pi T}{v}(v\tau \pm ix). \qquad (8)$$

In the case of $S=1$ HALC, on the other hand, it is difficult to map the corresponding Hamiltonian onto the $S=1/2$ XXZ model. However, according to Haga and Suga, by treating the power-decay terms as in the case of the $S=1/2$ dimerized chain and the $S=1/2$ ladder, and using the above conformal mapping, the temperature dependence of T_1^{-1} in this system is described in terms of the exponents η and η^z, apart from the geometrical factor, as follows;[10]
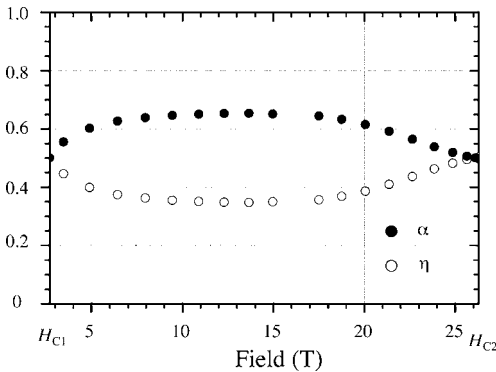
FIG. 5. Numerical calculation for the field dependence of η for the staggered mode and the exponent α of the relaxation rate with the relation of $\alpha=1-\eta$.[16]

$$\frac{1}{T_1} \propto C_\| T^{\eta_z-1} + D_\perp T^{\eta-1}, \qquad (9)$$

where the first and second terms result from the longitudinal incommensurate mode and the transverse staggered mode, respectively, and the coefficients $C_\|$ and $D_\perp$ are considered to be dependent only on the external field.

According to the numerical calculation for the field dependence of the exponents η and η_z given in Ref. 4, we find $\eta=1/2$ and $\eta_z=2$ at the vicinity of H_{C1} and H_{C2}, and $\eta \le 1/2$ and $\eta_z \ge 2$ for $H_{C1} \le H \le H_{C2}$. Thus, we may owe the experimental divergent behavior of T_1^{-1} to the second term in Eq. (9), that is, the transverse staggered mode. Thus, we have

$$\frac{1}{T_1} \propto D_\perp T^{-\alpha}, \qquad (10)$$

where $\alpha=1-\eta$.

Figure 5 shows the result for the recent numerical calculation for the field dependence of the exponent η performed for $N=20$ by Sakai by putting $H_{C1}=2.7$ T and $H_{C2}=27$ T so as to adopt to TMNIN.[16] As is seen, the power $\alpha=1-\eta$ increases, with increasing field, from 0.5 at H_{C1} up to the maximum value of 0.66 around the middle point $H=(H_{C1}+H_{C2})/2$.

Figure 6 shows the result of the fitting of the theoretical curves of Eq. (10), which were calculated using the values of α given in Fig. 5, to the experimental temperature dependence of T_1^{-1} for $H>H_{C1}$. The experimental results include the points presented in Fig. 2 and new results obtained for $H=6.8$ T. As is seen, the experimental results are compatible
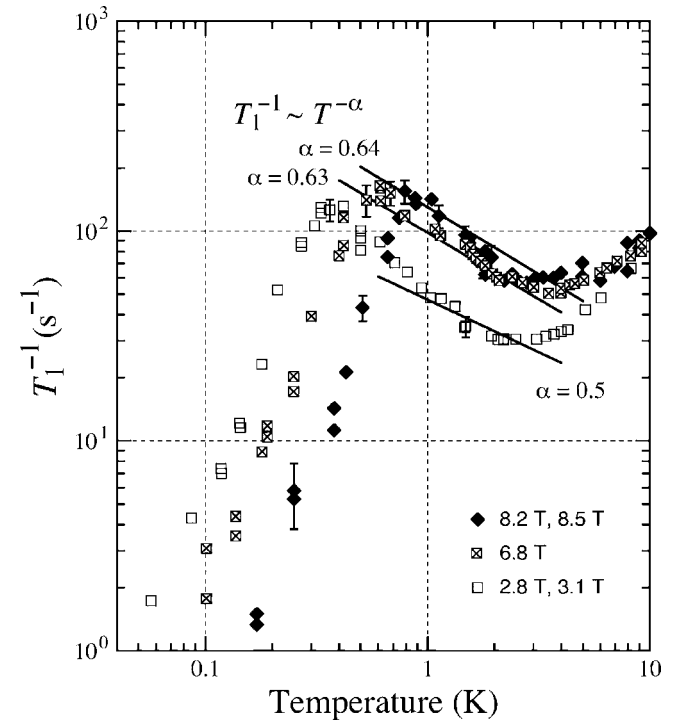
FIG. 6. Temperature dependence of T_1^{-1} for $H>H_{C1}$. The solid lines represent the curve of $T_1^{-1}\sim T^{-\alpha}$ for the TL phase, where the values of α are taken from Fig. 5.

with the expected values of the power α in Eq. (10) in the temperature range between the appearances of the round minimum and the round peak in T_1^{-1}. In view of this, we believe that our experimental result yields evidence for the realization of the TL liquid phase in the Haldane-gap system TMNIN. However, as for the results at $H=2.8$ T, the agreement between the experiment and the theoretical curve with a constant value of $\alpha \approx 0.5$ holds only down to about 1.2 K, and at lower temperatures T_1^{-1} has a trend to become somewhat remarkable. Though it is supposed that such a discrepancy may be related to the fact that the relevant field is just above H_{C1}, any further theoretical consideration is difficult at the moment. Furthermore, it is not certain how we find the consistency with the fact that the presence of a finite energy gap has been observed in the heat capacity measurement even for $H>H_{C1}$.[21]

As mentioned in Sec. I, the first experimental evidence for the TL liquid phase in the gapped system was found in the temperature dependence of T_1^{-1} of proton given by Eq. (10) in $S=1/2$ two-leg ladder system CuHpCl.[9] According to the numerical calculation for the power α in Eq. (10) for the exchange interactions in CuHpCl such that $J_\perp$ along the rung, which is antiferromagnetic, is much larger than $J_\parallel$ along the leg, the value of α takes the maximum of 0.5 at H_{C1} and H_{C2}, and decreases to 0.35 as the field departs from the critical fields.[11] However, the experimentally observed temperature dependence of T_1^{-1} seems, instead, to exhibit the qualitatively opposite behavior.[9] In the present case for $S=1$ HALC, the experimental results are consistent with the numerical evaluation for the $S=1$ HALC,[16] and $S=1/2$ two-leg ladder with ferromagnetic exchange interaction along the rung.[11]

With decreasing temperature, the relaxation rate T_1^{-1} changes into a remarkable decrease after taking a round peak. There appears a distinguished difference in the NMR spectrum at the temperatures above and below the peak of T_1^{-1}, and the peak temperature has a trend to increase with increasing field.

B. Gapped state

Next we look at the result for the gapped phase according to the theory presented by Sagi and Affleck.[17] For the first excited triplet state with three branches of $S_z=\mp 1$ and 0 for TMNIN, we assume the following dispersion relation for magnon as given in Ref. 17;

$$\epsilon_0(k) = \sqrt{\Delta^2 + (vk)^2} \approx \Delta + \frac{1}{2\Delta}(vk)^2, \qquad (11)$$

where k is wave vector with respect to twice of the lattice spacing along the c axis, and Δ is the energy gap at $k=0$, and $v=2JS$ with $S=1$. Here the single-ion anisotropy term D has been reasonably neglected. In the presence of the external field H, three branches are separated as

$$\epsilon_H(k) = \epsilon_0(k) + c(\alpha)g\mu_B H, \qquad (12)$$

where $c(\alpha)=-1$, $+1$, or 0, corresponding to $S_z=-1$, 1, or 0, respectively (see Fig. 7).
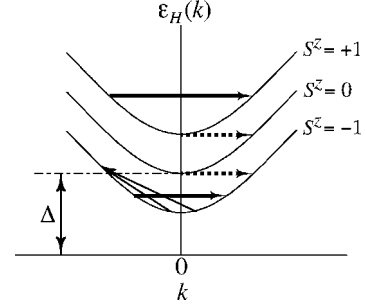
FIG. 7. Excitation spectrum for the $S=1$ HALC in the presence of the external field, which is expressed in terms of wave vector k with respect to twice of the lattice spacing along the c axis. The thick, dotted, and solid arrows indicate intrabranch, interbranch, and staggered processes, respectively.

Three types of relaxation processes are possible. These are intrabranch, interbranch, and staggered processes.[17] The intrabranch process occurs due to the magnon scattering within each of the $S_z=-1$ and 1 branches, which are referred to as lower and upper branches, respectively. The nuclear spin can relax by spin fluctuation accompanied by the magnon scattering between the states of wave vectors k and $k+q$, and $-k$ and $k+q$ with respect to fluctuating wave vector q. Then, the effective matrix elements in Eq. (3) are given by $\langle k+q|S_q^z|k\rangle$ and $\langle k+q|S_{q+2k}^z|-k\rangle$, where $q \approx 0$ because of the energy-conservation requirement. Unless the external field is low, the excitations with small values of k in the lower branch of $S_z=-1$ are effective because of the Boltzmann factor. However, as we see below, the effect of the upper branch of $S_z=1$ appears when the external field is low.

The relaxation process corresponding to the latter is schematically shown by the thick arrows in Fig. 7. There is no contribution from the $S_z=0$ branch, since the corresponding matrix element is 0. The use of the approximate dispersion relation of Eq. (12) yields, for the temperature range such that $\hbar\omega_N \ll k_B T \ll \Delta$, the following expression for T_1^{-1}:[17]

$$\left(\frac{1}{T_1}\right)_{\text{low(upp)}} = A \ln\left(\frac{4k_B T}{\hbar\omega_N} - \gamma\right)\exp\left(-\frac{\Delta \mp g\mu_B H}{k_B T}\right),$$

$$(13)$$

where the suffixes low and upp, and $\mp$ refer to the branches $S_z=-1$ and $S_z=1$, respectively, A is a prefactor corresponding to the coupling constant, and γ $(=0.577\ldots)$ is Euler constant. Then the total relaxation rate T_1^{-1} is given by the sum of contributions from the lower and upper branches. In high field region where $(T_1^{-1})_{\text{low}} \gg (T_1^{-1})_{\text{upp}}$, we find $T_1^{-1} \approx (T_1^{-1})_{\text{low}}$. In low field region, on the other hand, the contribution from the upper branch with the energy gap of $\Delta + g\mu_B H$ becomes effective, too, and then it is expected that the field dependence in T_1^{-1} diminishes because of the opposite contributions from the lower and upper branches with respect to the change in the external field.

The staggered process due to the transverse dynamical structure factor $S_\perp(q, \omega_N)$ is associated with magnon interactions. In the lowest process, three magnons are involved in each of the lower and upper branches in such a way that two
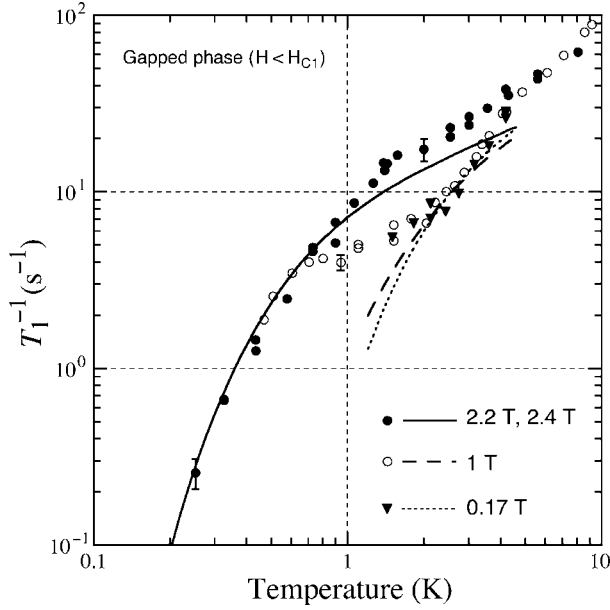
FIG. 8. Comparison between the experiment and the calculation for the intra branch process [Eq. (13) in the text] below $H < H_{C1}$. The value of the prefactor A is chosen so as to obtain the best fitting.

magnons are created (annihilated) and one magnon is annihilated (created) simultaneously. This gives rise to $S_{\perp}(q, \omega_N)$, where the relevant value of q is much larger than $q \approx 0$, as shown by the solid arrows in Fig. 7. The requirement for the energy conservation imposes the condition such that twice the minimum energy has to be smaller than the maximum energy. Then the relaxation rate is governed mainly by the square of the Boltzmann factor for the lowest branch, as expressed as

$$\frac{1}{T_1} \propto \exp\left[\frac{-2(\Delta - g\mu_B H)}{k_B T}\right]. \tag{14}$$

The interbranch process, on the other hand, occurs involving the magnon scattering between the different branches $S_z = 0$ and $S_z = -1$, or 1, which is associated with the transverse components S^x and S^y via the interacting term, like $I^+ S_j^-(t)$ in the perturbing Hamiltonian $\delta \mathcal{H}_{\text{dip}}$, as shown by the dotted arrows in Fig. 7. Because of the energy-conservation requirement, the gap energies that govern the relaxation process are Δ for $S_z = 0$ branch and $\Delta + g\mu_B H$ for $S_z = +1$ branch. The suppression by Boltzmann factor is more pronounced than that in the intrabranch process.

Now we examine our experimental results. The solid, dashed, and dotted lines in Fig. 8 represent the theoretical curves obtained from Eq. (13) by choosing a common prefactor so as to obtain the best fit to the experimental results for $H = 0.17 \sim 2.4$ T at low temperatures below about 4 K. The qualitative agreement between the experiment and the calculation is satisfactory. As is seen in Fig. 8, the temperature dependence of T_1 becomes almost field independent for $H < 1$ T. That is, the sum of contributions to T_1^{-1} from the upper and lower branches, remains almost the same regardless of the change in the external field. This is well under-

stood by considering that the field-dependent terms are given from Eq. (13) as $(T_1^{-1})_{\text{low(up)}} \propto \exp(\pm g\mu_B H / k_B T)$, where $\pm$ refer to the lower and upper branches, respectively. Note that such a situation is realized only when the single-ion anisotropy term D/k_B is negligibly small; thus, the zero-field splitting between the lower and upper branches is being neglected. Our result is consistent with other experimental results that give a very small value for the single-ion anisotropy. It is easily found that other two relaxation processes do not explain the experimental results because the relevant gap energies $2(\Delta - g\mu_B H)$ and Δ result in more remarkable temperature dependence of T_1^{-1}.

As we see in Sec. V, we may ascribe the hump of T_1^{-1} observed at $H = 1$ T to the fractional-spin effect in the $S = 1$ HALC. This is associated with effective end spin of $S = 1/2$, which cannot participate in the singlet pair called valence-bond-solid (abbreviated as VBS) in the finite chain. Then, as the resonance frequency increases, the peak of T_1^{-1} should move to the higher temperature and the corresponding peak value of T_1^{-1} becomes smaller. Thus, such a fractional-spin effect is not expected to appear for the higher fields, where the intrabranch relaxation process for the lower branch becomes more predominant because of reduction of the gap energy.

V. DISCUSSION

First we summarize various features obtained in the previous two sections in the temperature-field diagram of Fig. 9. We plotted the temperature for the round minimum in T_1^{-1} by a closed circle, which corresponds to the change from the $T\chi_0$ behavior to the $T^{-\alpha}$ behavior as given by Eqs. (6) and (10), respectively. The temperature range below the boundary obtained by connecting these points may be ascribed to the TL liquid phase in TMNIN. The open square in the figure represents the temperature where the round maximum in T_1^{-1} appears, and the plus sign represents the temperature where the broadening of the NMR spectrum and the change of its shape begin.

Here we refer briefly to the expected field-induced long-range order in the gapless phase of TMNIN. Sakai has revealed in his numerical study that the long-range order is caused by the presence of relatively weak inter-chain interaction J'.[22] The light solid line in Fig. 9 shows the phase boundary for the long-range order in the gapless phase of TMNIN, which is obtained by the calculation for lattice points of $N = 20$ assuming the interchain interaction $J' = 0.01 J$ and two critical-field values.[23] As is seen, the temperature for the boundary, which is of the order of 0.01 K, is much lower as compared to the temperature where the change in the NMR spectrum and the round peak of T_1^{-1} appear. Thus, we may suppose that the experimental features as above are not related to the field-induced long-range order. However, at present, the reason for this is not clear. On the other hand, in the case of proton NMR in the gapless phase of CuHpCl, appreciable shift in the spectrum and similar drastic change in the temperature dependence of T_1^{-1} have been observed, and the reason has been ascribed to the occurrence of the long-range order.[24] Probably, there is essen-
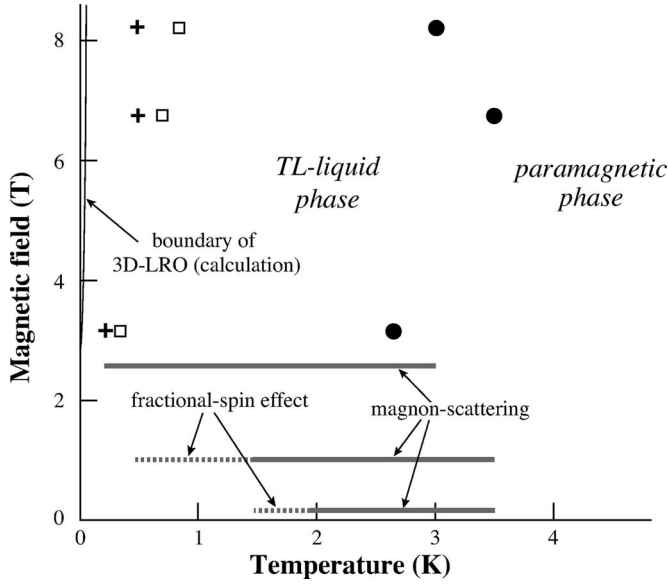
FIG. 9. The temperature-field diagram for various features in TMNIN revealed from the present relaxation measurements. The closed circles and the open squares indicate, respectively, the temperatures for the round minimum and the maximum of T_1^{-1} for the applied external fields. The light solid line represents the phase boundary for the 3D long-range order evaluated numerically by Sakai.[23] The plus sign represents the temperature where the increase and the change of the NMR spectrum begins.

tially different situations between the gapless phases of CuHpCl and TMNIN at low temperatures.

The heavy lines in Fig. 9 represent the temperature range where the relaxation mechanism due to the magnon scattering occurs. The dotted lines represent the temperature range where the fractional-spin effect in the nuclear magnetic relaxation emerges, on which we discuss below in some detail.

Next we shall look at the anomalous hump of T_1^{-1} observed at the low temperatures in low field region of the gapped phase below 1 T. In Fig. 10, we show typical examples of the recovery of normalized nuclear magnetization $m(t)$, which is defined in Sec. III. As is seen in Fig. 10(a), $m(t)$ does not exhibit single-exponential recovery as a whole in the low fields below about 1 T and at the low temperatures below 1 K. This is in contrast to normal single-exponential recovery of $m(t)$ observed over more than one decade for the other conditions as shown as a typical case in Fig. 10(b).

Previously, one of the present authors (T.G.) studied the same problem for the proton spin-lattice relaxation in pure Haldane-gap system $Ni(C_2H_8N_2)_2NO_2(ClO_4)$ (abbreviated as NENP) and Mg^{2+}-doped NENP,[25] and in Zn^{2+}-doped TMNIN.[26] Let us assume that there exist the fractional spins that do not participate in the constitution of the singlet-pair in the $S=1$ HALC. Then, as explained in Ref. 25, there appear two characteristic time constants T_1 and τ_1 in the recovery of normalized nuclear magnetization $m(t)$: During the initial short time after the saturation of the nuclear magnetization, $m(t)$ exhibits single exponential recovery as $m(t) = \exp(-t/T_1)$, and subsequently it follows $\sqrt{t}$ behavior as $m(t) = \exp(-\sqrt{t/\tau_1})$. These two time constants are given, respectively, as
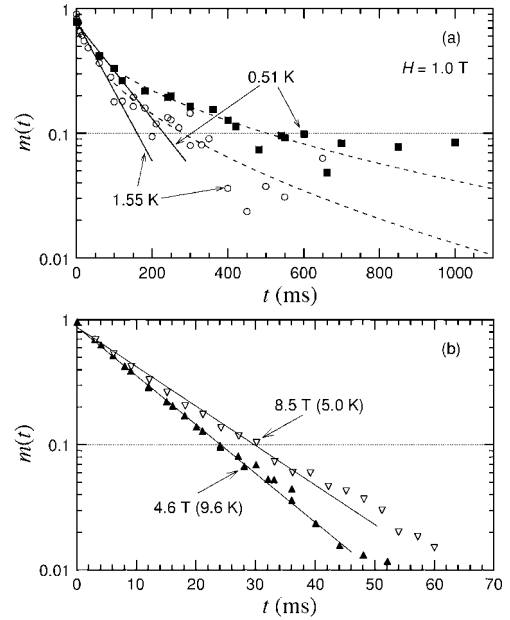
FIG. 10. Examples of the recoveries of the normalized nuclear magnetization $m(t)$ as functions of time t after the saturation the nuclear magnetization: (a) anomalous recovery for low fields below 1 T and the low temperatures below about 2 K, and (b) normal recovery. Straight lines in (a) and (b) correspond to the single exponential recoveries, which yield the time constants T_1, and the dotted lines in (a) represent the curve $m(t) = \exp(-\sqrt{t/\tau_1})$ with another time constant τ_1.

$$\frac{1}{T_1} = \frac{4\pi N_0 c_e C}{3 b_0^3} \quad (t < t_0), \tag{15}$$

and

$$\frac{1}{\tau_1} = \left(\frac{4 N_0 c_e}{3} \right)^2 \pi^3 C \quad (t > t_0), \tag{16}$$

with $t_0 = b_0^6/C$, where

$$C = \frac{2}{5} (g\mu_B\gamma_N)^2 S(S+1) \frac{\tau_e}{1 + \omega_N^2 \tau_e^2}. \tag{17}$$

Here τ_e is the longitudinal relaxation time of the fractional spin defined in the time-correlation given by $\langle S^z(t)S^z(0)\rangle = S^2 \exp(-t/\tau_e)$, and c_e, N_0 and b_0 are concentration of the fractional spin, density of the Ni^{2+} spins, and the exclusion radius, respectively. The exclusion radius is defined to be a radius of the sphere around one fractional spin, the nuclei within which are away from the resonance condition because of an appreciable internal field due to the corresponding magnetic moment. Thus $m(t)$ changes from single exponential into $\sqrt{t}$ behaviors around the time defined by t_0.

In view of this, we determined T_1 from the single-exponential recovery of $m(t)$ as indicated by the straight line given in Fig. 10(a), and τ_1 by plotting $m(t)$ as a function of $\sqrt{t}$ as given by the dashed lines in the figure.

In Fig. 11 the temperature dependence of T_1^{-1} and τ_1^{-1} below 1.7 K are plotted together with the normal relaxation rate at higher temperatures. As is seen, both of the two time
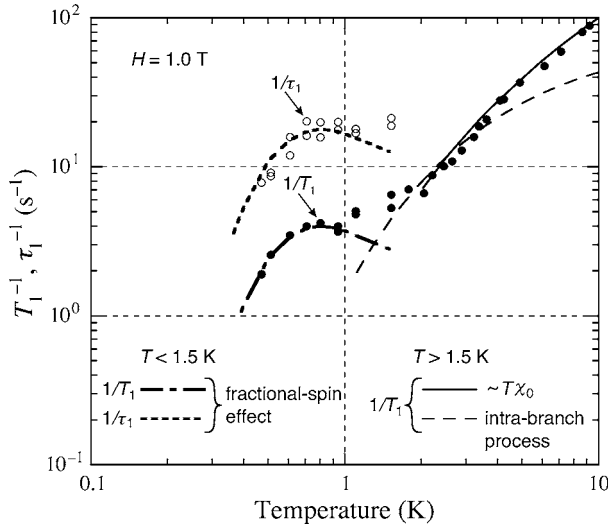
FIG. 11. Comparison between the experimental results at H =1 T and the theoretical treatment for the fractional-spin effect. The closed and open circles below 1.7 K indicate the inverses of the time constants T_1 and τ_1, which characterize the recovery of nuclear magnetization for the initial short-time and long-time durations, respectively. The dotted-dashed and dotted lines represent the theoretical curves for T_1^{-1} and τ_1^{-1} characterizing the fractional-spin effect, which were calculated respectively from Eqs. (15) and (16) using relevant numerical values given in the text. The closed circles above 1.7 K indicate usual relaxation rate. The solid and dashed lines represent the theoretical curves for the usual paramagnetic fluctuation and intrabranch process expressed by Eqs. (6) and (13), which have already been given in Figs. 4 and 8, respectively.

constants exhibit round humps at the same temperature.

By looking at the factor C in Eqs. (15) and (16), which is given by Eq. (17), it turns out that the humps of T_1^{-1} and τ_1^{-1} are realized when $\omega_N \tau_e = 1$. The relaxation time τ_e of the fractional spin is considered to be due to collision with the thermal Haldane excitations propagating on the linear chain.[27] Then we may tentatively put $\tau_e = \tau_0 \exp[\Delta'/(k_B T)]$, where Δ'/k_B represents the effective activation energy, and τ_0 is a prefactor. As the resonance frequency ω_N (or the applied field) increases, the value of τ_e for the hump decreases, the corresponding temperature increases, and the maximum value of T_1^{-1} becomes smaller. Since the relaxation rate for the intrinsic mechanism becomes more pronounced, it is not likely that the fractional spin effect appears at higher fields than about 1 T, as explained in Sec. IV. We can evaluate the concentration of the fractional spin c_e in the present TMNIN. Using the lattice constants, we obtain $N_0 = 3.94 \times 10^{21}/cm^3$. As for the exclusion radius, we apply $b_0 = 1.1 \times 10^{-7}$ cm determined in the case of NENP.[25] Then by comparing the experimental temperature dependence of T_1^{-1} to the above theoretical equation, we find $\Delta'/k_B = 1.5$ K, and $c_e = 2.2 \times 10^{-3}$. The temperature dependence of the two relaxation rates T_1^{-1} and τ_1^{-1} were evaluated using the above numerical values. The calculated results are represented in Fig. 11 by the dotted-dashed and dotted lines, respectively, together with the theoretical curves for the normal relaxation rates which have been already given in Sec. IV. The present value of c_e is reasonable in view of the value of $c_e = 1.0 \times 10^{-3}$ evaluated in

pure NENP.[25] It is noted that the experimental results for T_1^{-1} below about 2 K at 0.17 T suggest the appearance of the fractional-spin effect.

Finally, we comment on the NMR spectrum in the gapless phase. The proton nuclei is coupled with the surrounding average magnetic moments $g\mu_B \langle S_z \rangle$ of the Ni^{2+} ions directed along the external field via the dipolar interaction. According to the point-dipole model, the internal field is calculated by taking the sum of contributions over the appropriate number of the Ni^{2+}-ion sites. The present measurement was done using the polycrystalline sample, which involves many tiny pieces of the single crystal. Thus, the NMR spectrum should exhibit essentially a powder pattern associated with the dipolar-interaction tensor.

In order to obtain the shape of the NMR spectrum, we need knowledges of the value of $g\mu_B \langle S_z \rangle$ and position of the protons in the chemical unit cell. In the gapless phase, we can evaluate $g\mu_B \langle S_z \rangle$ from the total magnetization at low temperatures given in Ref. 15. For instance, for the measurement at $\nu_N = 286.7$ MHz in the gapless phase, which corresponds to the magnetic field of $H = 6.734$ T for the free proton nucleus, we obtained the value of $g\mu_B \langle S_z \rangle = 0.3\mu_B$. As for the position of the proton, since it is not definite in the crystal structure, the positions of the carbon sites in $(CH_3)_4 N$ ion were used instead.

Considering the present experimental situation for the polycrystalline sample, we randomly assumed 2000 kinds of orientations of the linear chain along the b axis with respect to the direction of the field-induced magnetic moments or the applied field. The calculation of the internal field was performed for each of the 2000 cases with respect to nonequivalent carbon sites in the unit cell by taking into account contributions including the neighboring unit cells, that is, $3 \times 3 \times 3$ unit cells as a whole. Then the intensity of the NMR signal was obtained by counting the number of carbon sites that feel the specified value of the internal field H_{int} within ± 0.0006 T, and the spectrum was obtained by plotting the intensity as a function of H_{int}.

The solid line in Fig. 3(b) represents the calculated NMR spectrum smoothed somewhat by the technique of convolution. This curve is shifted by about 0.01 T to the higher side so as to fit the peak position to the experimental value. The spectrum has a sharp peak, and there appear a round shoulder and another small shoulder on the left side of the line and a much smaller shoulder on the right side. The appearance of these shoulders corresponds to the two inequivalent carbon sites in the unit cell as shown in Fig. 1, which yield slightly different principal values of the dipolar tensor. As we see in Fig. 3(b), the calculated spectrum agrees qualitatively with the experimental spectrum taken at 0.68 K. However, the latter is much broader as compared to the former. Such a quantitative difference may be due to the crudeness of the calculation based on the point dipole model. In addition, since there are a larger number of inequivalent proton sites in the unit cell, it is probable that the experimental NMR spectrum actually becomes broader as compared to the above evaluation.

On the other hand, at lower temperatures where T_1^{-1} changes into a rapid decrease after taking the round peak, the

linewidth of the NMR spectrum exhibits appreciable increase. Such a change seems to be associated with the appearance of an alignment of the average magnetic moments at the Ni^{2+} sites, which may differ largely from the field-induced magnetic moments. The lack of the sharp anomaly in T_1^{-1} suggests that the change in the shape of the spectrum will not be due to occurrence of the long-range order. In fact, as indicated in Fig. 9, numerical calculation predicts the much lower ordering temperature, and there has not been observed any experimental evidence for the long-range order, for instance, in the heat capacity measurement.[21] One probable reason for the change in the NMR spectrum might be due to the appearance of staggered moments in the linear chain of TMNIN, as treated by Chiba *et al.* for the Haldane-gap system NENP, where the individual linear chain consists of two crystallographically inequivalent Ni^{2+} ions.[28] However, we do not have any clear knowledge for the reason at the moment.

VI. CONCLUSION

The proton spin-lattice relaxation in the $S=1$ Haldane-gap system $(CH_3)_4NNi(NO_2)_3$ (TMNIN) has been investigated in the gapless and gapped phases above and below the first critical field H_{C1} (=2.7 T). In the gapless phase, T_1^{-1} exhibited an appreciable increase with decreasing temperature below 3 K following to the equation $T_1^{-1} \sim T^{-\alpha}$, where the exponent α takes the value around 0.6. Such a feature was satisfactorily interpreted by the theoretical equation of $T_1^{-1} \sim T^{\eta-1}$, which is due to the staggered mode of the transverse

correlation with the power-law decay with respect to distance in a one-dimensional chain with exponent η. This yields an evidence for the realization of the Tomonaga-Luttinger liquid phase. At low temperatures below 1 K for the gapless phases, there appears a peak of T_1^{-1} and the change in the NMR spectrum. The reason for this is not clear at the present. In the gapped phase where T_1^{-1} decreases with decreasing temperature, the experimental features were well explained in terms of the intrabranch process associated with the scattering of the magnons within each of the $S^z=-1$ and $S^z=+1$ excited states. In relation to the relaxation rate at low fields below 1 T and low temperatures below about 2 K, the effect of the fractional spin has been observed. The concentration of the fractional spin in the present pure TMNIN was estimated to be 2.2×10^{-3} from the comparison between the experiment and the calculation.

*Electronic address: TakaoGoto@fm2.seikyou.ne.jp

†Present address: Canon Inc., Kanagawa 213-8512, Japan.

‡Electronic address: fujii@apphy.fukui-u.ac.jp

[1] F. D. M. Haldane, Phys. Rev. Lett. **45**, 1358 (1980).

[2] S. Tomonaga, Prog. Theor. Phys. **5**, 544 (1950).

[3] J. M. Luttinger, J. Math. Phys. **4**, 1154 (1963).

[4] T. Sakai and M. Takahashi, J. Phys. Soc. Jpn. **60**, 3615 (1991).

[5] T. Sakai, J. Phys. Soc. Jpn. **64**, 251 (1995).

[6] R. Chitra and T. Giamarchi, Phys. Rev. B **55**, 5816 (1997).

[7] T. Giamarchi and A. M. Tsvelik, Phys. Rev. B **59**, 11398 (1999).

[8] G. Chaboussant, P. A. Crowell, L. P. Lévy, O. Piovesana, A. Madouri, and D. Mailly, Phys. Rev. B **55**, 3046 (1997).

[9] G. Chaboussant, Y. Fagot-Revurat, M.-H. Julien, M. E. Hanson, C. Berthier, M. Horvatic, L. P. Lévy, and O. Piovesana, Phys. Rev. Lett. **80**, 2713 (1998).

[10] N. Haga and S. Suga, J. Phys. Soc. Jpn. **69**, 2431 (2000).

[11] M. Usami and S. Suga, Phys. Rev. B **58**, 14401 (1998).

[12] M. B. Stone, Y. Chen, J. Rittner, H. Yardimci, D. H. Reich, C. Broholm, D. V. Ferraris, and T. Lectka, Phys. Rev. B **65**, 064423 (2002).

[13] V. Gadet, M. Verdaguer, V. Briois, A. Gleizes, J. P. Renard, P. Beauvillain, C. Chappert, T. Goto, K. Le Dang, and P. Veillet, Phys. Rev. B **44**, 705 (1991).

[14] P. Gaveau, J. P. Boucher, T. Goto, L. P. Regnault, and J. P. Renard, J. Appl. Phys. **69**, 5956 (1991).

[15] T. Takeuchi, H. Hori, T. Yoshida, A. Yamagishi, K. Katsumata, J-P. Renards, V. Gadet, M. Verdaguer, and M. Date, J. Phys. Soc. Jpn. **61**, 3262 (1992).

[16] T. Sakai (private communication). The second critical field H_{C2} was taken to be 27 T instead of 30 T (Ref. 15). There is no essential difference.

[17] J. Sagi and I. Affleck, Phys. Rev. B **53**, 9188 (1996).

[18] G. Chaboussant, M.-H. Julien, Y. Fagot-Revurat, L. P. Lévy, C. Berthier, M. Horvatic, and O. Piovesana, Phys. Rev. Lett. **79**, 925 (1997).

[19] L. -K. Chou, K. A. Abboud, and D. R. Talham, J. Magn. Magn. Mater. **104-107**, 813 (1992).

[20] G. E. Granroth, L.-K. Chou, W. W. Kim, M. Chaparala, M. J. Naughton, E. Haanappel, A. Lacedrda, D. Rickel, D. R. Talham, and M. W. Meisel, Physica B **211**, 208 (1995).

[21] T. Kobayashi, A. Kohda, K. Amaya, M. Ito, H. Deguchi, K. Takeda, T. Asano, Y. Ajiro, and M. Mekata, J. Phys. Soc. Jpn. **63**, 1961 (1994).

[22] T. Sakai, Phys. Rev. B **62**, R9240 (2000).

[23] T. Sakai (private communication).

[24] H. Mayaffre, M. Horvatić, C. Berthier, M.-H. Julien, P. Ségransan, L. Lévy, and O. Piovesana, Phys. Rev. Lett. **85**, 4795 (2000).

[25] T. Goto, S. Satoh, Y. Matsumura, and M. Hagiwara, Phys. Rev. B **55**, 2709 (1997).

[26] T. Goto, S. Sato, K. Kitamura, N. Fujiwara, J. P. Renards, and M. W. Meisel, J. Magn. Magn. Mater. **177-181**, 663 (1998).

[27] P. P. Mitra, B. I. Halperin, and I. Affleck, Phys. Rev. B **45**, 5299 (1992).

[28] M. Chiba, Y. Ajiro, H. Kikuchi, T. Kubo, and T. Morimoto, Phys. Rev. B **44**, 2838 (1991).